

Shape and Model from Specular Motion

Jiang Yu Zheng, Yoshihiro Fukagawa and Norihiro Abe

Faculty of Computer Science and Systems Engineering
Kyushu Institute of Technology,
Iizuka, Fukuoka 820, Japan

Abstract

This work investigates visual characteristics of specular surfaces during rotation, and gives approaches to qualitatively identify and quantitatively recover shapes of these surfaces. Continuous images are taken when an object rotates. We look at specularly reflected patterns on the surfaces and their motion in the EPIs parallel to the rotation plane, from which estimation of each surface point and construction of the object model are carried out. We find very simple and direct methods to fulfill this objective; linear equations for multiple lights illumination, and a 1st-order differential equation for single light illumination. The motion of specular reflection has nice global characteristics in EPI. The surface types range from very shiny metal surfaces to surfaces with only weak specular reflectance. We give both simulation and experiments on real objects.

1. Introduction

The current techniques of 3D shape measure in vision can not deal with specular surface successfully. Even laser range finder could not get the correct shape of a surface with strong specular reflectance because the projected laser stripe will be reflected away. But in the real world, there are plenty of objects from industrial parts to daily goods containing specular reflectance. The objective of this work is to estimate 3D shapes of specular surfaces by rotating them.

It is well known that for a specular surface, motion of surface texture differs from motion of reflected patterns of environment when the view point shifts. This is a cue used by human in perceiving specularity. Conventional shape from motion approach is no longer applicable here. For a shiny surface, surrounding environment is visible on it. For a weak specular surface with strong illuminants around, highlights may appear on it. Some effort has been made to remove highlights [7,8]. However, in the case where few texture appears on the surface, reflected patterns and highlights play an important rule in the perception of surface shape.

To simplify the problem, we use orthogonal projection such that visible features and their properties are not related to viewing distance but only related to viewing angle of the camera. We only consider the relative rotation of objects with respect to the camera, which is an intrinsic

case in dealing with specular motion. In order to recover a complete model, we put the object on a turn table and rotate it so that it reveals all of its surfaces to the camera.

The motion information is taken from Epipolar-Plane Images (EPI) [5] parallel to the rotation plane. Two kinds of visual features ----- fixed features either from corners or textures, and points of specular reflection including highlights are considered to use. The reflecting points gradually shift on object surfaces during the rotation. Their motion can be tracked in EPIs at different heights. From the obtained motion trajectories, object surfaces are calculated on each rotation plane.

In this paper, we will give both qualitative and quantitative results of shape recovery. Qualitatively, we will classify surface shapes on the rotational plane into corner, convex, planar and concave types by referring global motion styles of the reflected patterns. The points where curvature changes from convex to concave can also be located directly.

Quantitatively, we estimate surfaces from motion trajectories of reflecting points. The shape on each rotation plane is estimated and a whole model is then constructed by connecting the shapes. Surface normal at a point with specular reflection is determined from the directions of ambient light and the camera. For a surface with strong specular reflectance, patterns in the environment are reflected. This corresponds to the case where the surface reflects multiple lights. If more than two lights are available, we obtain redundant measures of surface points and their average can be computed. If only two reflected lights are possible to be found, we still can compute shape directly by linear equations. For a surface containing weak specular reflectance, multiple strong lights around can produce highlights on it. The shape recovery is just the same as above. If a single light is set, we estimate surface by a first-order differential equation which has unique solution [6]. Combining those fixed features as its boundary condition, we can finally reconstruct the model.

The contributions on the specularity so far include separation of defused and specular reflectance components [7,8], computation of surface normals [10], and analysis of specular disparity and specular motion from several images which constrains surface shape [3,11]. There has no direct computation of object shape using highlights yet.

2 Environment Analyses

2.1 Experimental System and Illumination

The system for experiment is displayed in Fig. 1. An object is put on the table and rotated. Its continuous images are taken under orthogonal projection and a spatial-temporal volume is piled. Through a simple calibration, the y axis of the image frame can be set parallel to the rotation axis and the optical axis of camera goes through the rotation axis. A surface point $\mathbf{P}(X, Y, Z)$ described in the object centered coordinate system O-XYZ is projected as $p(x, y, \theta)$ in the volume. The rotation angle θ is known and is clockwise in the analysis (Fig. 2).

Ambient lights are assumed to be vertically extended (Fig. 1). It is described by a distribution $L(\phi)$ where ϕ is the angle from the camera direction (Fig. 3). Points on the same rotation plane hence catch the same ambient lights during the rotation even their normals might be different in the y direction. Each part of ambient light could be either a real vertical illuminant or a long vertical object, which is not difficult to realize in the real indoor environment. Ambient lights are located far away compared with the object scale so that the horizontal components of incident rays reaching different parts of object are parallel (orthogonal illumination from each light). The whole ambient lights can be denoted by their angle ϕ , which is $L=L(\phi)(-\sin\phi, \cos\phi)$ and $\phi \in (-\pi, \pi)$ in the camera coordinate system C-XZ.

2.2 Geometry of Camera, Light and Normal

As an object rotates, a surface point has its trace in the EPI as a sinusoidal curve (half visible period), even it is not distinct enough to be located. One example of EPI is shown in Fig. 4, in which an object with both concave and convex shapes rotates. Patterns are painted on its surfaces to yield dark traces. From the camera geometry (Fig. 2), we know the viewing direction under orthogonal projection is $\mathbf{v} = (-\sin\theta, \cos\theta)$ in the system O-XZ. The image position of a visible point at the camera angle θ can be written as

$$\mathbf{x}(\theta) = \mathbf{P} \cdot \mathbf{x} = X(\theta) \cos\theta + Z(\theta) \sin\theta \quad (1)$$

where \mathbf{x} is the unit vector of the horizontal image axis.

Obviously, the position reflecting an ambient light from ϕ shifts on surfaces during the rotation. The angle of incidence is equal to the angle of reflection there. Therefore, the surface normal is at angle $\phi/2$ in the system C-XZ and the angle of the normal is written as $\kappa = \theta - \pi/2 + \phi/2$ in the system O-XZ. We obtain an equation describing the surface normal as

$$(X_{\theta}', Z_{\theta}') \cdot (\cos\kappa, \sin\kappa) = 0 \quad (2)$$

where $(X_{\theta}', Z_{\theta}')$ is the tangent direction at the reflecting point. It is further written as

$$(X_{\theta}', Z_{\theta}') \cdot (-\sin(\theta + \phi/2), \cos(\theta + \phi/2)) = 0 \quad (3)$$

2.3 Photometric Properties

In the coordinate system O-XZ, the angle of reflection at a specular point is $r (= \kappa - \pi/2 - \theta)$ and the angle of incidence is $i (= \pi/2 + \theta + \phi - \kappa)$. Under one illuminant, the intensity reaching the camera can be expressed by surface reflectance and intensity of the light, i.e.

$$\begin{aligned} I(\theta, \kappa) &= L(\phi) (S(\theta, \kappa) + D(\theta, \kappa)) \\ &= L(\phi) (\cos^S((r+i)/2 - r) + D \cos i) \end{aligned} \quad (4)$$

where D and S are coefficients of diffused and specular reflectances respectively. As shown in Fig. 5, the diffused reflectance under one light is a sinusoidal function of i (Fig. 5(b)), which becomes brightest when $i=0$. When the point is back to the light, $I(\theta, \kappa)$ becomes dark even during the visible period of camera. The specular reflection, however, appears as a strong peak when $i=r$ and has small values elsewhere (Fig. 5(c)). The composite effect is shown in Fig. 5(d).

In the same way, we can deduce the reflectance under a distribution of ambient lights (Fig. 6). As a result, the diffused reflection at a point is the integral of reflections from each part of the distribution, i.e.

$$D(\kappa, \theta) = \int_{-\pi/2}^{\pi/2} L(\phi) \cos i d\phi \quad (5)$$

The surface may have positive intensities in all visible directions of the camera. A specular surface point, however, only reflects a single part of the ambient lights at a time. If we set

$$i = r \quad (6)$$

we can deduce that in the system O-XZ, the reflected ambient light is from $\phi = 2\kappa - 2\theta - \pi$, which means

$$S(\kappa, \theta) = L(2\kappa - 2\theta - \pi) \quad (7)$$

When the θ increases, the surface point reflects in turn each part of ambient lights. The ambient light distribution $L(\phi)$ is hence mapped onto the sinusoidal trace of the point in the EPI as the distribution of specular reflection.

2.4 Multiple Lights and Single Light Modes

In order to deal with the problem in a proper mathematical way, we separate the physical environment of observation into three different cases ----- multiple lights, two lights and single light.

If specular reflectance is the dominant component, we get a shiny surface which reflects patterns in the ambient world. It corresponds to multiple lights reflected from the surface, although there might have no real illuminant around. We focus on edges reflected from vertical edges in the environment, since they provide locatable position information.

If specular reflectance is not strong enough to reflect all of the surroundings, but does reflect some strong illuminant, it yields highlights on the surface. We can put more than two, and two vertical lights around to produce the circumstance of multiple lights.

If two lights are available, we will give shape of surface on the rotational plane by solving a two dimensional linear equation. If more than two patterns or lights exist, redundant processing can even improve the accuracy of the surface.

If, on the other hand, only one light is set for a surface with weak specular reflectance (single light mode), the shape can be obtained by computing an integral which is the unique solution of a first-order differential equation.

3. Qualitative inference of Shapes

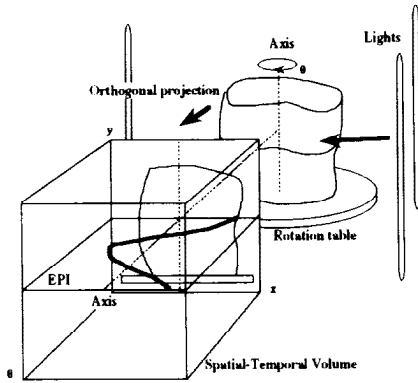


Fig. 1 Image formation geometry.

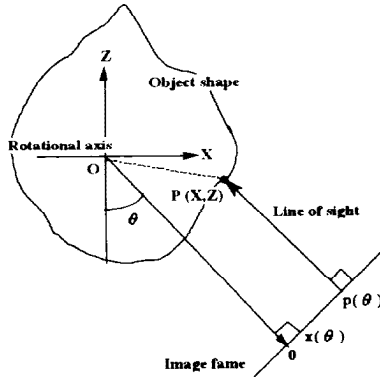


Fig. 2 One cross section of an object parallel to the rotation plane.

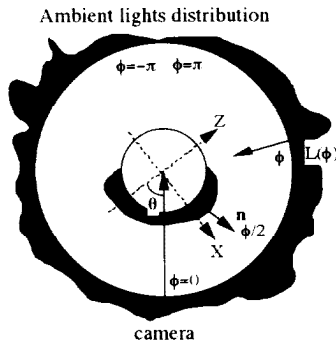


Fig. 3 Ambient light distribution illuminates rotational objects.

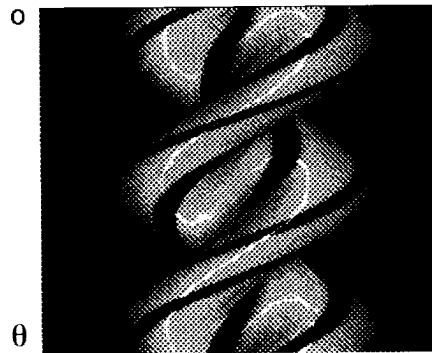


Fig. 4 One example of EPI of rotational object.

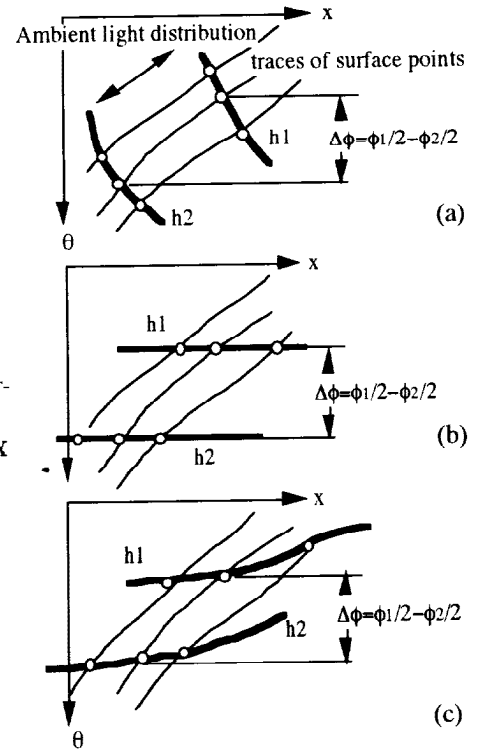


Fig. 8 Delay of a surface point in reflecting two particular lights. (a) convex, (b) plane (c) concave. h1 and h2 denote two highlight traces.

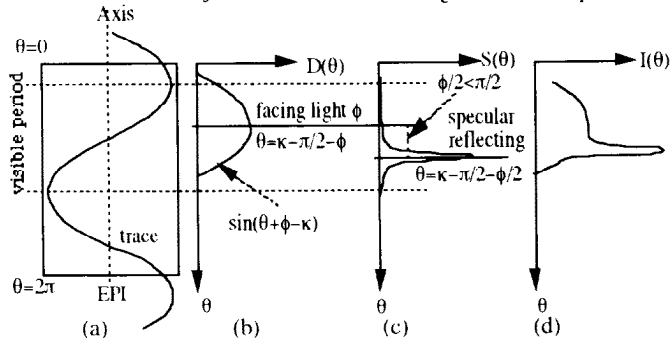


Fig. 5 Specular and diffused reflectance at a surface point under one illumination. (a) trajectory of the point in the EPI. (b) diffused reflectance change along the trajectory of the point. (c) specular reflectance on the trajectory of the point. (d) composite effect of reflectance.

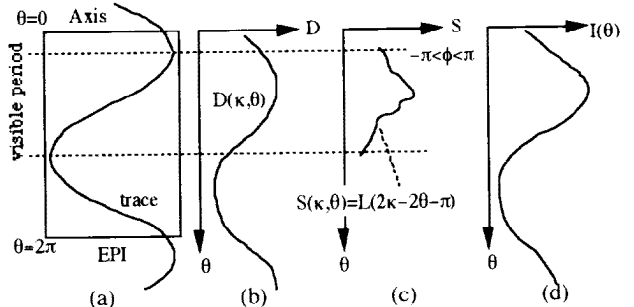


Fig. 6 Specular and diffused reflectances under a distributed ambient lights. (a) trajectory of a point in the EPI. (b) diffused reflectance changes along the trajectory of the point. (c) specular reflectance on the trajectory of the point. (d) composite effect of reflectance.

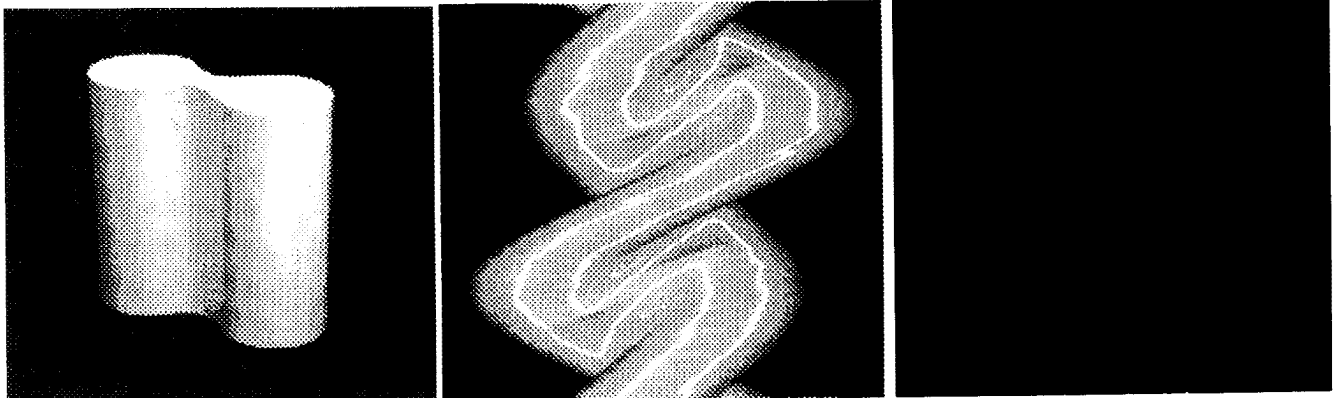


Fig. 11 A real object with concave shapes and one of its EPI. (a-left) object. (b-middle) one of its EPI. Interreflection produced traces are closed curves with weak intensity. They do not intersect with the traces of directly reflected lights. (c-right) extracted traces of highlight.

3.1 Motion Characteristics of Fixed Points

If the surface normal component in the rotation plane is discontinuous at a point (corner), the shadings between its two sides are different. Its trace in EPI appears typically as a segment of sinusoidal curve. Moreover, if the surface albedo has a discontinuity at a point (edge of surface pattern), the point also draws a sinusoidal trace in the EPI. These two kinds of surface points become fixed points since they have no relative motion to the surface while they are being observed. The image velocity of a fixed point in the EPI is then a cosine function to the left. From tracked trajectories of fixed points, we can obtain their 3D positions by using shape from motion method. Also, we can verify if a tracked trajectory of edge is from a fixed point by checking whether the trace is a sinusoidal curve starting from the right contour trace and finishing at the left one. The traces of fixed points will be used as the reference of traces of specular points.

3.2 Qualitative Motion of a Specular Point

In order to qualitatively infer the shape, let us look at the motion types of a specular point in the EPI. As an object rotates, its surface elements, in turn, face to each part of surrounding patterns. The specular point reflecting a particular ambient light shifts on the surfaces. This move means the image velocity of the specular point is different from that of surface points. If a bright light or an edge of environment is reflected from the shiny surface, its trajectory is possible to be located in the EPI during the rotation.

According to curvature along the object boundary in a horizontal cross section, shapes are categorized as either one of convex corner, convex, linear, concave, concave corner, which have curvature as $+\infty$, $+$, 0 , $-$, and $-\infty$, respectively. They produce different motions of the specular point in the EPI. Figure 7 shows relative moves of reflected lights on three boundaries (Fig. 7(a)) and the corresponding trajectories over traces of surface points in the EPIs (Fig. 7(c)). According to the categorized shapes, segments and points on the boundaries are labeled. The same labels are attached to the corresponding traces of fixed points and specular reflecting points in the EPIs.

A linear boundary (zero curvature) has its surface points face a light at the same time, which generates a horizontal stripe of reflected light at a particular angle of θ . Finding horizontal stripes in the EPI (for example, E, F, G, H in Fig. 7.1(c)), we can identify planar shapes on the boundary. Extending this result, those absolute points where curvature changes from convex to concave or in reverse should have horizontal traces of zero length in the EPI. Finding these changing points (A, B, C, D in Fig. 7.2(c) and A, B in Fig. 7.3(c)), we can separate a trace of specular point into segments moving on convex and concave shapes.

On a convex shape, the reflected light keeps staying on the camera and light side during the rotation. Its image velocity is lower than that of the surface points (its trace crosses traces of surface points, as F, H in Fig. 7.2(c) and

C, D, F in Fig. 7.3(c)). A concave shape, however, the reflecting point moves in the same direction with the surface points; its image velocity is higher than that of the surface points. The point has a trace crossing traces of surface points (E, G in Fig. 7.2(c) and E in Fig. 7.3(c)). If a trace is segmented by two points where curvature changes sign, we can assert the segment is either convex or concave on the rotation plane by checking how it crosses with a trace of surface pattern (a visible case of surface point). Across the two end points, the segments on the other side must be concave or convex.

As the absolute value of curvature becomes high, the shape is close to a corner. The motion of a reflected light there is close to that of surface points (C, D in Fig. 7.3(c)). At an ideal corner ($+\infty$ curvature), highlight does not appear (A, B, C, D in Fig. 7.1(c)). Similarly, a concave corner ($-\infty$ curvature) has the same effect. Therefore, those corner traces (other than traces of surface pattern) connect traces of specular points in the EPI.

The above analysis can also be applied locally rather than to the whole rotation sequence. If we want to know the combination of different surfaces, a longer image sequence is necessary. During the rotation, specular points split and merge, appear and disappear at zero curvature points, and move along convex and concave surfaces. The surface connection can also be recognized from the specular trajectories in EPI [6].

As a result, a reflecting point shifts on object surfaces and passes all surface points at least once if no occlusion of light occurs. With either fixed or shifting points on object surfaces, a queue of connected trajectories in EPI crosses trajectories of all surface points in one period of rotation. We hence attempt to compute positions of all surface points from this queue.

3.3 Motion of Multiple Specular Points

If a surface has strong specular reflectance, or multiple vertical lights are set around, multiple reflected patterns or lights are visible. From Eq. 3, we understand when the normal of a surface point rotates to angle $\phi/2$, the point reflects pattern of environment from angle ϕ in the system C-XZ. According to the analysis in Fig. 6, a surface point in turn reflects each part of $L(\phi)$ during the camera visible period. Hence, the visible range of the normal ($-\pi/2, \pi/2$) reflects almost the whole surrounding patterns $\phi \in (-\pi, \pi)$. For a shiny point, the distribution of ambient lights is squeezed by half of the angle ϕ and appears as specular reflection along its sinusoidal trace in the EPI (Fig. 3).

For two lights at ϕ_1 and ϕ_2 , a point will reflect them when its normal is at angles $\phi_1/2$ and $\phi_2/2$ in the system C-XZ; having a delay $\Delta\phi = \phi_1/2 - \phi_2/2$. This delay holds for concave, linear, and convex shapes as depicted in Fig 8. Because of the delay, two traces of specular points reflecting different lights will never cross with each other in the EPI. At either concave or convex corner, these traces merge together into a corner trace. Figure 9 shows a simulation which displays traces of multiple lights

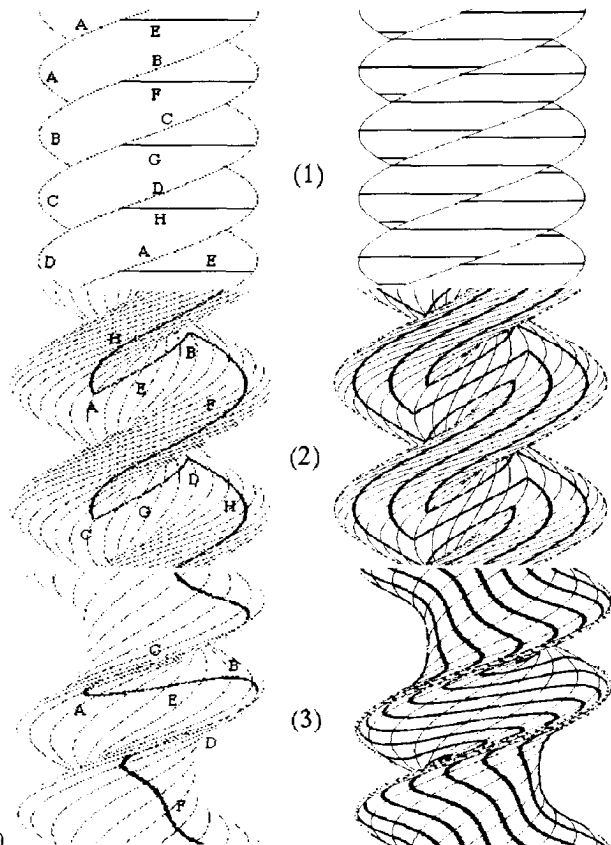
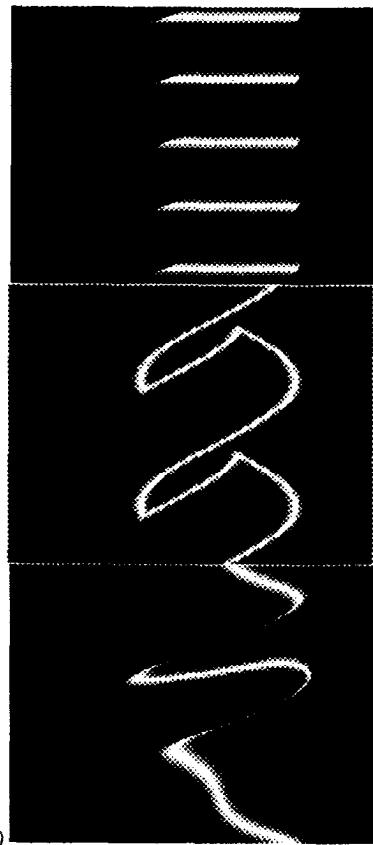
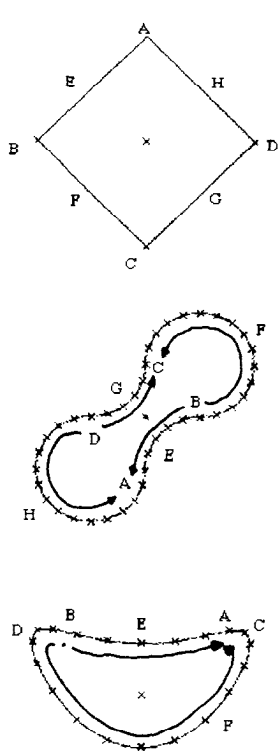


Fig. 7 Simulated results of surface point traces and traces of a reflected light (a vertical linear light) when objects rotate clockwise. (a) three kinds of shapes containing corner, convex, concave and linear shapes (surface points are marked with * sign, rotation axis is with x sign). The camera axis is the same as the Z axis at the beginning. The motion of specular points on the shapes are also depicted. (b) EPIs. Both specular reflectance and diffused reflectance exist. The light direction ϕ is 60 degree on the right of the camera. (c) traces of surface points (narrow curves) from those with * sign and the traces of reflected light (bold curves).

Fig. 9 Traces of surface points and traces of multiple reflected lights. The shapes generating (1) (2) (3) are the same as those in Fig. 7.

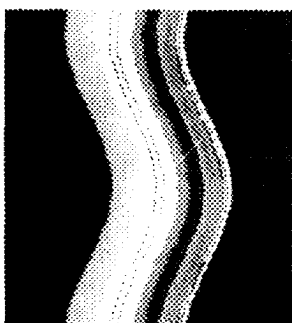
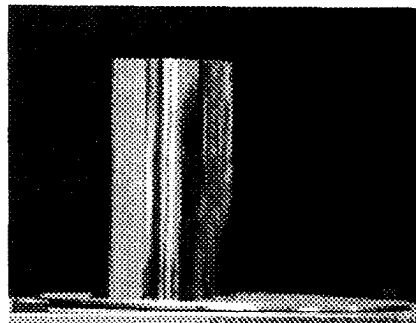


Fig. 10(a) Fig. 10(b)

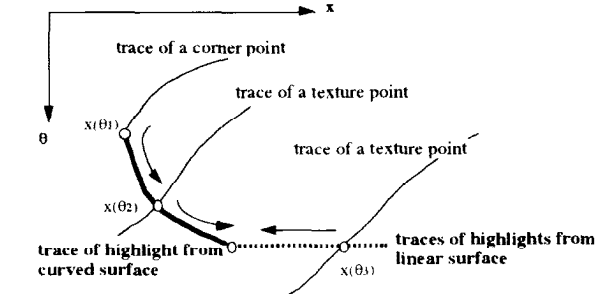


Fig. 12 Estimation of smooth shape starting from fixed points.

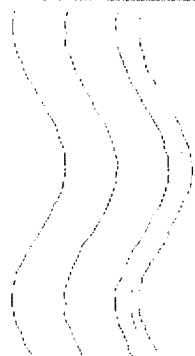


Fig. 10(c)

Fig. 10 Reflected patterns of environment from an object with shiny surface. (a) object. (b) one of its EPI. (c) tracked traces of points reflecting edges of ambient light distribution.

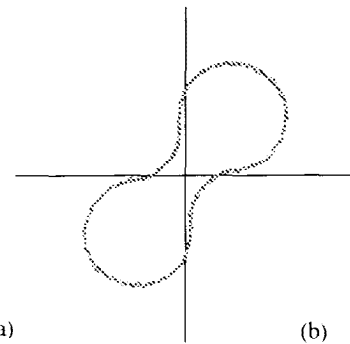
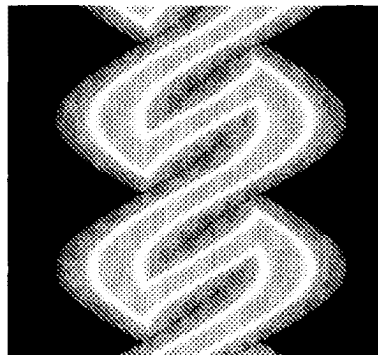


Fig. 13 A simulated EPI and the recovered shape under two lights illumination.

reflected from the same boundaries as in Fig. 7. The intervals between lighting angles are 40 degree for Fig. 9(1) and Fig. 9(2), 30 degree for Fig. 9(3), respectively.

Although multiple traces of reflected lights will not cross, their density depends on curvature of boundary. The density becomes high when the absolute value of curvature is great (shape close to a corner).

4 Shape Recovery with Multiple Lights

4.1 Two Lights

As analyzed in the previous section, if two vertical lights are set at ϕ_1 and ϕ_2 , a surface point will in turn reflect them when its normal rotates to $\phi_1/2$ and $\phi_2/2$ in the camera coordinate system. At the first direction, we have an equation from the camera geometry as Eq. 1, i.e.

$$x_1(\theta) = X(\theta) \cos \theta + Z(\theta) \sin \theta \quad (8)$$

where $x_1(\theta)$ is the image position of the point (X, Z) reflecting the first light. After a duration $\Delta\phi = (\phi_1 - \phi_2)/2$, the point reflects the second light, which gives

$$x_2(\theta + \Delta\phi) = X(\theta) \cos(\theta + \Delta\phi) + Z(\theta) \sin(\theta + \Delta\phi) \quad (9)$$

From the two equations, the surface point (X, Z) can be directly computed by

$$\begin{pmatrix} X(\theta) \\ Z(\theta) \end{pmatrix} = \frac{1}{\sin \Delta\phi} \begin{pmatrix} \sin(\theta + \Delta\phi) & -\sin \theta \\ -\cos(\theta + \Delta\phi) & \cos \theta \end{pmatrix} \begin{pmatrix} x_1(\theta) \\ x_2(\theta + \Delta\phi) \end{pmatrix} \quad (10)$$

We only need to track two traces which are reflection of two lights at known directions. For each point at one trace, we pick up the point at the second trace which has the delay $\Delta\phi$ from the first one. The geometry explanation of Eq. 10 is as follows. Being constrained by two ambient lights, two lines of sight which view the specular point at two particular angles cross each other at the surface point so that the position of the point is determined.

4.2 Multiple Lights

If more than two lights are reflected by a smooth surface, we have multiple measures of the same surface by combining each two traces of reflected lights. That means we have redundant data and we can average them to produce more accurate position. Suppose the multi-lights are at the angle $\phi_1, \phi_2, \phi_3, \dots, \phi_n$ in the system C-XZ. Similar as the two lights case, we can write a series of linear equations, each corresponds to a line of sight through the same surface point. The equations are

$$x_1(\theta) = X \cos \theta + Z \sin \theta \quad (11)$$

$$x_2(\theta + \Delta\phi_2) = X \cos(\theta + \Delta\phi_2) + Z \sin(\theta + \Delta\phi_2)$$

$$\dots\dots\dots x_i(\theta + \Delta\phi_i) = X \cos(\theta + \Delta\phi_i) + Z \sin(\theta + \Delta\phi_i)$$

$$\dots\dots\dots x_n(\theta + \Delta\phi_n) = X \cos(\theta + \Delta\phi_n) + Z \sin(\theta + \Delta\phi_n)$$

where $\Delta\phi_i = (\phi_1 - \phi_i)/2$ and $i=1, \dots, n$. Now that we have n equations for only two unknowns (X, Z) , we can use the least squared error method to compute the point (X, Z) , which is finally given by

$$\begin{pmatrix} X(\theta) \\ Z(\theta) \end{pmatrix} = \left[\frac{n^2}{2} - \frac{1}{2} \left(n + 2 \sum_{k < j} \cos 2(\phi_j - \phi_k) \right) \right]^{-1} \times$$

$$\begin{pmatrix} -\sum_{i=1}^n \sin 2(\theta + \Delta\phi_i) & n - \sum_{i=1}^n \cos 2(\theta + \Delta\phi_i) \\ n + \sum_{i=1}^n \cos 2(\theta + \Delta\phi_i) & -\sum_{i=1}^n \sin 2(\theta + \Delta\phi_i) \end{pmatrix} \times \begin{pmatrix} \sin(\theta + \Delta\phi_1) & \dots & \sin(\theta + \Delta\phi_n) \\ \cos(\theta + \Delta\phi_1) & \dots & \cos(\theta + \Delta\phi_n) \end{pmatrix} \begin{pmatrix} x_1(\theta + \Delta\phi_1) \\ \vdots \\ x_n(\theta + \Delta\phi_n) \end{pmatrix} \quad (12)$$

In this equation, the first three parts without unknown x_i are computed only once after knowing the number and angles of ambient lights.

If the surface is very shiny, there has no need to put many lights around. The edges in $L(\phi)$ where a prompt change exists are also visible on the object surface, and in turn draw their traces in the EPIs. We can focus on the edges and follow their traces in EPI to compute surface point using Eq. 12. Figure 10 gives an example of a mirror-like metal surface. The traces in one of its EPI are visible due to the reflection of environment.

4.3 Lights Calibration and Interreflection

The location of multiple lights $L(\phi)$ can be obtained either from system setting or through a very simple calibration. To locate ambient lights, we first put a planner mirror at the center of the table and rotate it. An EPI is generated from this standing mirror. The range where the mirror reflects ambient lights to the camera is $\theta \in (-\pi/2, \pi/2)$, which catches $L(\phi)$ in $\phi \in (-\pi, \pi)$. If an edge of $L(\phi)$ exists at ϕ , there must be a horizontal edge appearing at angle $\phi/2$ in the EPI. Extracting horizontal edges in the EPI using a vertical edge operator, we can understand locations of edges as well as their contrasts in the ambient space $L(\phi)$. Two lights case is even simple. Any zero curvature point (appears on plane) on the test object will have a delay in reflecting two lights, which yields two horizontal segments on the two traces of highlights respectively. Measuring the difference of θ between the two segments gives the angles of two lights.

One problem needed to discuss is interreflection on a concave surfaces. It does exist during the rotation. Figure 11 shows an EPI taken from a real object with concave shapes. Under the multiple lights, however, it is interest to notice that the traces due to interreflection are closed curves near concave shape generated traces in the EPI. Such traces will not intersect with traces of directly reflected lights. Moreover, if the reflected patterns are real lights, the intensity of the traces due to the second reflection are weak because the energy has been reduced. It is possible to filter them out in highlights detection.

5 Shape Recovery with a Single Light

5.1 Shape Recovery from a Highlight

If the surface has weak specular reflectance and only one strong vertical light is set, we can observe a highlight on the object surface. At any instance, the line of sight through the highlight also satisfies Eq. 1. Assuming the shape is not linear, the corresponding highlight trace is

then not horizontal and we can take derivative of Eq. 1 with respect to θ to obtain

$$x'(\theta) = X\theta'\cos\theta + Z\theta'\sin\theta - X\sin\theta + Z\cos\theta \quad (13)$$

The first two terms express a possible shift of highlight on the surface and $(X'\theta, Z'\theta)$ gives the tangent direction of the boundary. From Eq. 1, Eq. 3 and Eq. 13, two differential equations

$$\begin{aligned} \frac{\partial Z}{\partial \theta} \cos \frac{\phi}{2} + Z \frac{\sin(\theta + \phi/2)}{\cos \theta} \\ = \frac{\partial x}{\partial \theta} \sin\left(\theta + \frac{\phi}{2}\right) + \sin \theta \sin\left(\theta + \frac{\phi}{2}\right) \frac{x}{\cos \theta} \end{aligned} \quad (14)$$

$$\begin{aligned} \frac{\partial X}{\partial \theta} \cos \frac{\phi}{2} - X \frac{\cos(\theta + \phi/2)}{\sin \theta} \\ = \frac{\partial x}{\partial \theta} \cos\left(\theta + \frac{\phi}{2}\right) - \frac{x \cos \theta}{\sin \theta} \cos\left(\theta + \frac{\phi}{2}\right) \end{aligned} \quad (15)$$

can be deduced in the domains $\theta \neq \pi/2$, $3\pi/2$, and $\theta \neq 0, \pi$, respectively. These θ angles are singular points and the equations diverges there. We use Eq. 14 within $[-\pi/4, \pi/4]$ and $[\pi-\pi/4, \pi+\pi/4]$, and use Eq. 15 within $[\pi/2-\pi/4, \pi/2+\pi/4]$ and $[3\pi/2-\pi/4, 3\pi/2+\pi/4]$ separately to avoid inaccurate description near the singular points. After $Z(\theta)$ or $X(\theta)$ is obtained, $X(\theta)$ or $Z(\theta)$ are computed by Eq. 1 accordingly. It is clear that Eq. 14 and Eq. 15 have unique solutions [6].

If, on the other hand, a boundary is linear, multiple points become highlights at the same angle θ so that taking derivative of $x(\theta)$ with respect to θ is impossible. There are multiple values of $x(\theta)$ along a horizontal line in EPI. Nevertheless, a linear segment can be determined in an even simple way [6].

5.2 Boundary Conditions for the Solutions

The boundary condition for the solutions of Eqs. 14,15 are from positions of fixed points which are very accurate [9], as well as contours if there is no single fixed point available.

A trajectory of corner connects trajectories of highlights. While a trajectory of texture point intersects a highlight trajectory without breaking it (Fig. 12). At end points of highlight trace and those crossing points, 3D positions become known. From these points, we start estimation of smooth boundary by computing integrals along highlight traces in EPIs. This process is done until a singular point with infinite $x'(\theta)$ (the trace has horizontal tangent) is reached. We need to change the direction of integral there for further propagation of shapes.

How to obtain position of a fixed point? We can compute it from a short segment of its trace in the EPI. Differentiating Eq. 1 with respect to θ and using constraint of fixed point

$$(X'\theta, Z'\theta) = (0, 0) \quad (16),$$

we obtain its position

$$\begin{aligned} X &= x \cos \theta - x'\theta \sin \theta \\ Z &= x \sin \theta + x'\theta \cos \theta \end{aligned} \quad (17)$$

which means the position can be estimated from $x(\theta)$ and the tangent direction of its trace at θ . The computation can be carried out many times along its trace so that fusion of multiple measures to yield a more accurate result is possible. We use the least squared estimation after the whole trace points are collected[9]. The estimation not only gives positions at nonsmooth parts, but also serves as boundary conditions for estimation of remaining parts.

6. Tracking Features in EPIs

Let us examine how traces of features in the EPIs can be extracted for shape recovery. For fixed points from pattern edges and corners, an ordinary edge detecting operator filters EPI both horizontally and vertically to obtain their locations. For a shiny surface, the operator also picks up edges reflected from the environment. To detect highlights, a ridge type operator is used horizontally and vertically to find locations with maximum intensity.

However, using these filters and picking up points with high response is not enough to identify entire traces of fixed points and highlights. Although taking high value from the ridge operator can ignore interreflection, it will miss highlight traces on dark surfaces, since the intensity is also related to the value of surface albedo. Similarly, the trace of a corner point is unable to be detected if the ambient light is homogeneous. Even a dominant light exist, the corner is invisible at where its contrast changes sign during the rotation. An edge pattern may disappear when it rotates to the back side of the illumination. However, those detecting modules will not fail at the same situation so we have chance to use them properly to produce complete traces.

Assume diffused reflectances on both sides of a texture point are R_1 and R_2 , and the surface normal has component $n_p(\theta)$ in the rotation plane. The difference of image intensities between two sides of the point is

$$\Delta I(\theta) = (R_1 - R_2) \mathbf{n}(\theta) \cdot \mathbf{L}(\phi) \quad (18)$$

The most distinct angle for tracking edge is when the point faces the light.

We first follow traces of fixed points in the EPI. Edges near the ridge operator output are removed since they should be edges of highlight. A set of tracked points are tested to see if they are from a fixed point by computing the error of the least square estimation. If the error is small, the fixed point is verified and its position is measured. Although the trace of a corner point may break, the 3D positions calculated from its two fragments are coincident so that the trace is connected again into a complete one. The remaining traces of edges may be moving points such as specular points. We then track reflecting points and highlights starting from places where outputs from the ridge operator are maximum.

7. Experimental Results

We have done experiments on simulated objects and real objects. Figure 13(a) displays a simulated EPI and traces of two reflected lights, from which the shape on the

rotational plane is correctly computed (Fig. 13(b)). For a real object in Fig. 11(a), the camera is at about 2.5m away from the rotation table and a lens with long focal length is used. A tracked EPI is given in Fig. 11(c) and the estimated model by connecting shapes at each rotational plane is shown in Fig. 14. The difference between the two light directions ($\Delta\phi$) are measured from delay at two horizontal segments of the highlight traces (Fig. 11(c)). We also test a real bottle, which gives the result in Fig 15. The shape is estimated at each rotational plane and the model is connected by many graphics patches.

Under a single light, we have obtained object models with convex and planar surfaces[6]. As to objects with concave shapes, Figure 16 displays the recovered model of the object in Fig. 11 using a single highlight and computing the integrals.

In the EPIs of real objects, we can find some nonsmoothness along the traces of specular points (Fig. 11). A short horizontal segment on highlight trace shows the existence of a short linear shape. This is not easy to be extracted from other visual cues such as disparity, motion, and contour directly, which implies specular reflection is also good for accurate shape measurement. Because there is no fluorescent light with infinite length in the real situation, a circular illumination is being considered to allow a point with large y component in its normal reflecting highlight to the camera.

8. Conclusion

In this paper, we described a new method for qualitative identification and quantitative recovery of shapes with specular reflectance. We control object rotation and detect motion of specular points including highlights, from which object surface can be computed at each point. Two methods proposed are very simple, which are direct computation without using regularization. We have worked on constructing 3D models of real objects from their specular motion, which has not been tried so far. The

experiment results verifies the correctness of our analysis and the applicability of the methods. The future work is to model more complicated objects and fuse specular information with other visual cues to produce models of various objects.

References

- [1] J.Y. Zheng, "Acquiring 3D models from sequences of contours", IEEE PAMI, Vol.16, No.2, Feb. pp.163-178, 1994.
- [2] J. Y. Zheng, and F. Kishino, "Verifying and combining different visual cues into a complete 3D model", CVPR92, pp. 777-780, 1992.
- [3] A. Black, G. Brelstaff, "Geometry from specularities", 2nd ICCV, pp.394-403, 1988.
- [4] P. K. Horn, "Shape from shading" The MIT Press 1989.
- [5] H. Baker, and R. Bolles, "Generalizing epipolar-plane image analysis on the spatiotemporal surface", CVPR-88, pp 2-9, 1988
- [6] J. Y. Zheng, Y. Fukagawa, T. Ohtsuka, N. Abe, "Acquiring 3D models from rotation and a highlight", 12th ICPR, Vol. 1, pp. 331-336, 1994.
- [7] G. Klinka, S. Shafer and T. Kanade, "The measurement of highlights in color images", IJCV, Vol. 2, No. 1, pp.7-32, 1988.
- [8] R. Gershon, A. D. Jepson, and J. K. Tsutsos, "Highlight identification using chromatic information", 1st ICCV, pp.161-171, 1987.
- [9] J. Y. Zheng, H. Kakinoki, K. Tanaka, N. Abe, "Acquiring 3D models from fixed points during rotation", ICARCV '94, Vol. 1, pp. 459-463, 1994.
- [10] K. Ikeuchi, "Determining surface orientations of specular surfaces by using the photometric stereo method", -----.
- [11] A. Zisserman, P. Giblin and A. Blake, "The information available to a moving observer from specularities", -----.
- [12] G. Healey and T. Binford, "Local shape from specularity".
- [13] R. Szeliski, "Shape from rotation", CVPR91, pp. 625-630, 1991.

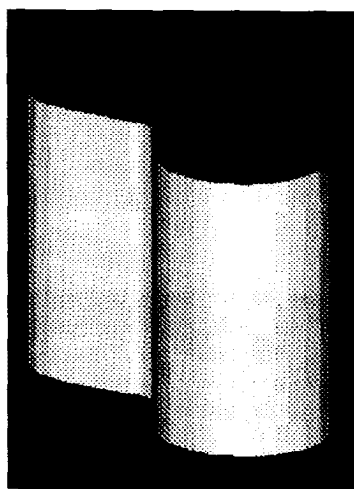


Fig. 14 Recovered model of the real object given in Fig. 11 under two highlights.

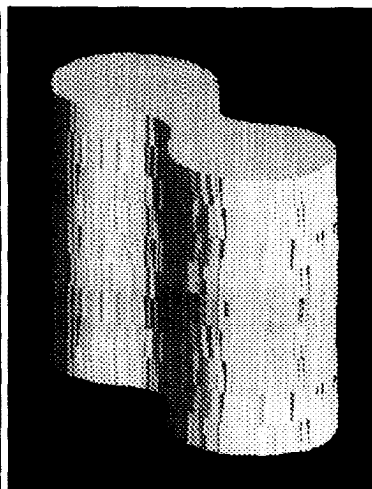


Fig.16 Recovered model of the object given in Fig. 11 under a single highlight.

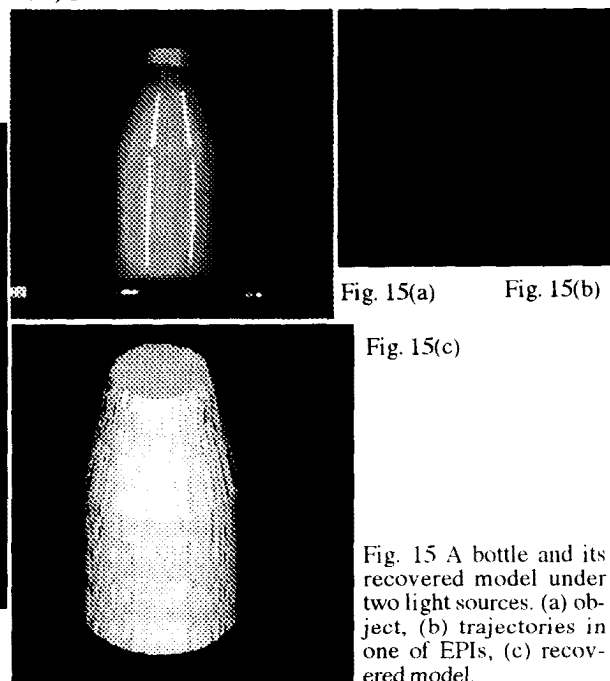


Fig. 15(a) Fig. 15(b)

Fig. 15(c)

Fig. 15 A bottle and its recovered model under two light sources. (a) object, (b) trajectories in one of EPIs, (c) recovered model.